Vol. 14, pp. 13–22 (2017)
doi: 10.2142/biophysico.14.0_13

Biophysics and Physicobiology
https://www.jstage.jst.go.jp/browse/biophysico/

Regular Article

Kinetic characteristics of chimeric channelrhodopsins implicate the molecular identity involved in desensitization

Alemeh Zamani[1,3,*], Shigeo Sakuragi[1,*], Toru Ishizuka[1] and Hiromu Yawo[1,2]

[1]*Department of Developmental Biology and Neurosciences, Tohoku University Graduate School of Life Sciences, Sendai, Miyagi 980-8577, Japan*
[2]*Center for Neuroscience, Tohoku University Graduate School of Medicine, Sendai, Miyagi 980-8575, Japan*
[3]*Present address: Okinawa Institute of Science and Technology Graduate University OIST, Onna-son, Okinawa 904-0495, Japan*

Received July 19, 2016; accepted December 29, 2016

Channelrhodopsin (ChR)-1 and ChR2 were the first-identified members of ChRs which are a growing subfamily of microbial-type rhodopsins. Light absorption drives the generation of a photocurrent in cell membranes expressing ChR2. However, the photocurrent amplitude attenuates and becomes steady-state during prolonged irradiation. This process, called desensitization or inactivation, has been attributed to the accumulation of intermediates less conductive to cations. Here we provided evidence that the dark-adapted (DA) photocurrent before desensitization is kinetically different from the light-adapted (LA) one after desensitization, that is, the deceleration of both basal-to-conductive and conductive-to-basal transitions. When the kinetics were compared between the DA and LA photocurrents for the ChR1/2 chimeras, the transmembrane helices, TM1 and TM2, were the determinants of both basal-to-conductive and conductive-to-basal transitions, whereas TM4 may contribute to the basal-to-conductive transitions and TM5 may contribute to the conductive-to-basal transitions, respectively. The fact that the desensitization-dependent decrease of the basal-to-conductive and conductive-to-basal transitions was facilitated by the TM1 exchange from ChR2 to ChR1 and reversed by the further TM2 exchange suggests that the conformation change for the channel gating is predominantly regulated by the interaction between TM1 and TM2. Although the exchange of TM1 from ChR2 to ChR1 showed no obvious influence on the spectral sensitivity, this exchange significantly induced the desensitization-dependent blue shift. Therefore, the TM1 and 2 are the main structures involved in two features of the desensitization, the stabilization of protein conformation and the charge distribution around the retinal-Schiff base (RSB^+).

Key words: optogenetics, photocycle, photocurrent, inactivation, spectral shift

Channelrhodopsin (ChR)-1 and ChR2 are the first-identified members of ChRs which are a growing subfamily of microbial-type rhodopsins [1–4]. Each molecule consists of seven transmembrane helices (TM1–7) with a covalently bound retinal as a chromophore [5–7]. In the case of ChR2, the basal state with all-*trans* retinal (D480) is non-conductive to

* These authors contributed equally to this work.
Corresponding author: Hiromu Yawo, Department of Developmental Biology and Neuroscience, Tohoku University Graduate School of Life Sciences, 2-1-1 Katahira, Aoba-ku, Sendai, Miyagi 980-8577, Japan.
e-mail: hiromu.yawo.c7@tohoku.ac.jp

◀ ***Significance*** ▶

Channelrhodopsins are desensitized during prolonged irradiation of light. Zamani *et al.* provided evidence that the desensitized photocycle is kinetically distinct and both rates from basal to conductive and conductive to basal states are decelerated during desensitization. Using channelrhodopsin-1/2 chimeras, they revealed that the transmembrane helices, TM1 and TM2, were the determinants of both basal-to-conductive and conductive-to-basal transitions, whereas TM4 may contribute to the basal-to-conductive and TM5 may contribute to the conductive-to-basal transitions, respectively. TM1 and 2 are the main structures involved in two features of the desensitization, the stabilization of protein conformation and the charge distribution around the retinal-Schiff base (RSB^+).

©2017 THE BIOPHYSICAL SOCIETY OF JAPAN

any ions. Light absorption is followed by the photoisomerization of the all-*trans* retinal to the 13-*cis* configuration and drives cyclic conformational changes of the molecule, called a photocycle, which consists of several intermediates such as P520, an intermediate conductive to cations. Consequently, very rapid (in the orders of ms) generation of a photocurrent is induced in cell membranes expressing ChR2. However, the photocurrent amplitude attenuates in the order of 10 ms and becomes a steady-state during prolonged irradiation [2,8,9]. This transition, which is termed desensitization or inactivation, has been attributed to the accumulation of intermediates less conductive to cations [6,7,10].

C1C2, one of the ChR1/2 chimeras, which consists of the N-terminal five domains of ChR1, each of which has a single TM, and the C-terminal counterpart domains of ChR2, is the first and only ChR the detailed structure of which has been crystallographically investigated [5]. However, the molecular dynamics involved in the desensitization has not been revealed since the molecule in a desensitized condition is hard to be crystalized. On the other hand, desensitized and non-desensitized photocycles can be differentiated by their photocurrent kinetics. In the present study, we compared the kinetics and spectral sensitivity between the desensitized and non-desensitized photocurrents of the ChR1/2 chimeras. The results suggest that the translocation of TM1 is involved in the kinetics and spectral change of ChR during desensitization.

Materials and Methods

Plasmids

The cDNAs encoding channelrhodopsin (ChR)-1 (ChR1, Met^{1}–Glu^{345}) and -2 (ChR2, Met^{1}–Lys^{315}) with 5′-EcoRI and 3′-BamHI restriction sites were prepared by conventional PCR and subcloned in-frame into pVenus-N1 [8]. Chimeric ChRs between ChR1 and ChR2 were prepared by overlap extension PCR and subcloned into pVenus-N1 [11,12], where the amino acid sequences of the ChRs were divided into seven domains so that each domain practically contained a single TM (Supplementary Fig. S1). These segments are referred to (from N-terminal to C-terminal) as "*A*," "*B*," "*C*," "*D*," "*E*," "*F*," and "*G*" for ChR1. The homologous counterparts of ChR2 are referred to as "*a*," "*b*," "*c*," "*d*," "*e*," "*f*," and "*g*." The N-terminal domain of ChR2 was replaced in order with the corresponding counterpart of ChR1 and we prepared 6 chimeras; ChR-*Abcdefg* from domain "*A*" (Met^{1}–Thr^{117}) of ChR1 and domain "*b*"–"*g*" (Cys^{79}–Lys^{315}) of ChR2, ChR-*ABcdefg* from domain "*A*" and "*B*" (Met^{1}–Leu^{164}) of ChR1 and domain "*c*"–"*g*" (Leu^{126}–Lys^{315}) of ChR2, ChR-*ABCdefg* from domain "*A*"–"*C*" (Met^{1}–Tyr^{184}) of ChR1 and domain "*d*"–"*g*" (Ser^{146}–Lys^{315}) of ChR2, ChR-*ABCDefg* from domain "*A*"–"*D*" (Met^{1}–Val^{212}) of ChR1 and domain "*e*"–"*g*" (Lys^{174}–Lys^{315}) of ChR2, ChR-*ABCDEfg* from domain "*A*"–"*E*" (Met^{1}–Val^{242}) of ChR1 and domain "*f*" and "*g*" (Pro^{203}–Lys^{315}) of ChR2, ChR-*ABCDEFg* from domain "*A*"–"*F*" (Met^{1}–Phe^{269}) of ChR1 and domain "*g*" (Ile^{231}–Lys^{315}) of ChR2. All constructs were verified by sequencing.

Cell culture

The electrophysiological assays of the ChRs were made using ND 7/23 cells, hybrid cell lines derived from neonatal rat dorsal root ganglia neurons fused with mouse neuroblastoma [13]. ND 7/23 cells were grown on poly-L-lysine (Sigma-Aldrich, St Louis, MO)-coated coverslip in Dulbecco's modified Eagle's medium (DMEM, Wako Pure Chemical Industries, Osaka, Japan) supplemented with 10% fetal bovine serum (Biological Industries, Kibbutz Beit-Haemek, Israel) under a 5% CO_2 atmosphere at 37°C. The cells were maintained for no more than ten passages and grown to 80%–90% confluence in the culture dish. The expression plasmids were transiently transfected in ND 7/23 cells using Effectene Transfection Reagent (Qiagen, Tokyo, Japan) according to the manufacturer's instructions. The medium was replaced with one supplemented with 2.5 μM all-*trans* retinal at 6 h after transfection. Electrophysiological recordings were then conducted 24–48 h after the transfection. Successfully transfected cells were identified by the presence of Venus fluorescence.

Electrophysiology

All experiments were carried out at room temperature (23±2°C). Photocurrents were recorded using an EPC-8 amplifier (HEKA Electronic, Lambrecht, Germany) under a whole-cell patch clamp configuration. The data were filtered at 0.7 kHz, sampled at 100 kHz (Digidata1440 A/D, Molecular Devices Co., Sunnyvale, CA) and stored in a computer (pClamp10.3, Molecular Devices). The pipette resistance was adjusted to be 2–5 MΩ (3.5±0.1, n=72) with a series resistance of 2.4–15 MΩ (7.6±0.3, n=72) and a cell capacitance of 17–56 pF (35±1, n=72). The series resistance was electrically compensated by 50%. As a result, the charging time constant was 130±6 μs (range, 33–302, n=72) after compensation.

The internal pipette solution for the whole-cell voltage clamp recordings from the ND 7/23 cells contained (in mM) 120 CsOH, 100 glutamate, 5 EGTA, 50 HEPES, 2.5 $MgCl_2$, 2.5 MgATP, 0.1 Leupeptin and 0.01 Alexa 568, adjusted to pH 7.3 with CsOH. The standard extracellular Tyrode's solution contained (in mM): 138 NaCl, 3 KCl, 2.5 $CaCl_2$, 1.25 $MgCl_2$, 10 HEPES, 4 NaOH, and 11 glucose (pH 7.4 adjusted with HCl).

Using software (pClamp10.3, Molecular Devices), the turning-on (ON) kinetics of each photocurrent was fitted by a single-exponential function for the transition phase between 10% and the peak of the maximal amplitude of photocurrent during irradiation. For the tuning-off (OFF) kinetics, the photocurrent transient after irradiation was fitted by a single-exponential function for the transition between 90 and 10% of the amplitude at the end of irradiation. Generally, no obvi-

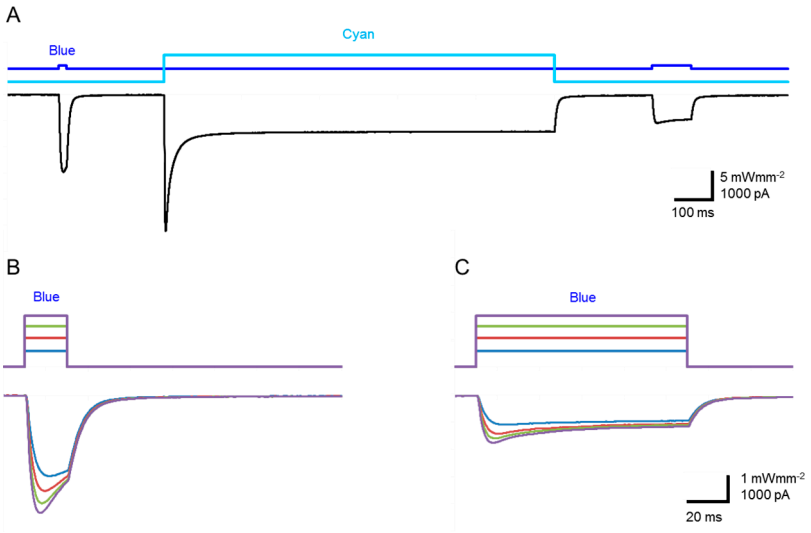

Figure 1 The differentiation of the dark-adapted (DA) and light-adapted (LA) kinetics of channelrhodopsin-2 (ChR2) photocurrent. (A) Sample trace of ChR2 photocurrent (bottom trace) evoked by two test pulses (upper blue trace, 20 and 100 ms) of light with blue (438±24 nm, 0.58 mWmm^{-2}) before and after irradiation of 1-s cyan light (middle cyan trace, 475±28 nm, 5.1 mWmm^{-2}), which completely desensitized the photocurrent. (B) The DA photocurrent with blue of variable irradiance (0.58, 1.1, 1.5 and 1.9 mWmm^{-2}). (C) The LA photocurrent with blue of variable irradiance (0.58, 1.1, 1.5 and 1.9 mWmm^{-2}).

ous deviation was observed between the raw data and the fitted curve (Supplementary Fig. S2). However, samples were not included in the statistics if their transients were deviated from the single exponential function.

Optics

To investigate the photocurrent kinetics, irradiation was carried out using a SpectraX light engine (Lumencor Inc., Beaverton, OR) controlled by computer software (pCLAMP 10.3, Molecular Devices) at wavelengths (nm, >90% of the maximum): 438±24 (blue), 475±28 (cyan) and 513±17 (teal). The power of the light was directly measured under a microscope by using a visible light-sensing thermopile (MIR-101Q, SSC Co., Ltd., Kuwana City, Japan). Every photocurrent was measured with a holding potential of −60 mV and at pH 7.4 outside. Two test pulses of light (20 ms and 100 ms) were applied before and after irradiation of 1-s strong light (blue: 438±24 nm, 5.1 mWmm^{-2} or cyan: 475±28 nm, 5.1 mWmm^{-2}). Each irradiation protocol was applied every 60 s to enable full recovery from the desensitization.

Statistical analysis

All data in the text, figures and tables are expressed as mean±SEM and were evaluated with the Wilcoxon signed rank test for statistical significance for paired data and with the Mann-Whitney *U*-test for unpaired data unless otherwise noted. It was judged as statistically insignificant when $P>0.05$.

Results

Desensitization-dependent changes of ChR2 kinetics

When ChR2 was expressed in ND 7/23 cells, the light evoked a photocurrent with a transient peak and a steady-state plateau (Fig. 1A). To distinguish the photocurrent kinetics of the desensitized photocycle from the non-desensitized one, two test pulses of light (20 ms and 100 ms) were applied to measure the photocurrents immediately before and after irradiation of 1-s strong light (blue: 438±24 nm, 5.1 mWmm^{-2} or cyan: 475±28 nm, 5.1 mWmm^{-2}) which completely desensitized the photocurrent. The test pulses of various colors of light were applied at various intensities: blue: 438±24 nm (0.58, 1.1, 1.5 and 1.9 mWmm^{-2}), cyan: 475±28 nm (0.35, 0.72, 1.1 and 1.4 mWmm^{-2}), teal: 513±17 nm (0.47, 0.81, 1.1 and 1.3 mWmm^{-2}). The ON and OFF transients of the first test pulse of light (20 ms, Fig. 1B) should be largely dependent on the photocycle kinetics of the non-desensitized ChR because of the relatively slow process of desensitization (time constant >20 ms) [14]. However, the fraction of desensitized ChR should increase over time during the test pulse. In the present paper, the ON and OFF time constants of the first test pulse of light (20 ms) are respectively referred to as the dark-adapted ON time constant, τ_{ON}(DA), and the dark-adapted OFF time constant, τ_{OFF}(DA), to distinguish them from the genuine kinetic parameters of non-desensitized ChR. On the other hand, the ON and OFF transient of the second test pulse of light (100 ms, Fig. 1C) was mostly dependent on the photocycle kinetics of the desensitized ChR because of the relatively slow recovery from desensitization (time constant >10 s) [2,8,9]. Even so, the fraction of non-desensitized ChR2

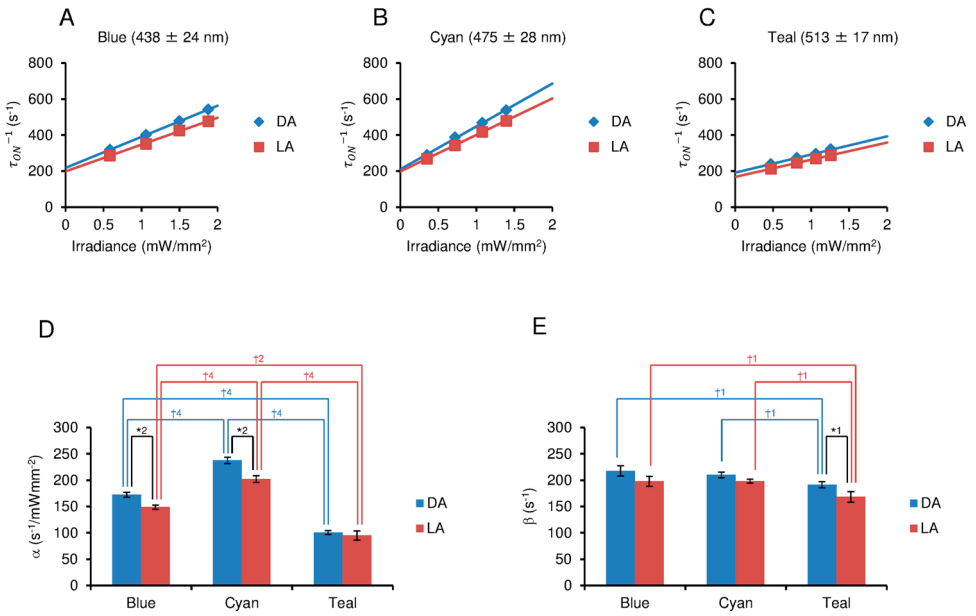

Figure 2 Desensitization-dependent changes of the ON kinetics. (A)–(C) The relationship between the ON rate constant (τ_{ON}^{-1}) and the irradiance of the DA (blue symbols) and LA (red symbols) photocurrents with blue (A, n=10), cyan (B, n=10) and teal (C, n=10). (D) The comparison of the slopes to the irradiance (α_{DA} and α_{LA}) between DA and LA photocurrents with blue (n=10), cyan (n=10) and teal (n=10). (E) The comparison of the light-independent constant (β_{DA} and β_{LA}) between DA and LA photocurrents with blue (n=10), cyan (n=10) and teal (n=10). Wilcoxon signed rank test: $*^1$ ($P<0.05$), $*^2$ ($P<0.005$) and Mann-Whitney *U*-test: $\dagger^1$ ($P<0.05$), $\dagger^2$ ($P<0.005$), $\dagger^4$ ($P<0.00005$).

should increase over time during the gap of 250 ms before the second test. In the present paper, the ON and OFF time constants of the second test pulse of light (100 ms) are respectively referred to as the light-adapted ON time constant, τ_{ON}(LA), and the light-adapted OFF time constant, τ_{OFF}(LA), to distinguish them from the genuine kinetic parameters of the desensitized ChR.

As shown in Figure 1B and C, the photocurrents peaked earlier with the increase of irradiance (power of light). Actually, each ON rate constant of the DA and LA photocurrents, τ_{ON}^{-1}(DA) and τ_{ON}^{-1}(LA), experimentally followed a linear function of the irradiance (*L*) (Fig. 2A). That is,

$$\tau_{ON}^{-1}(DA) = \alpha_{DA}L + \beta_{DA}, \quad (1)$$

and

$$\tau_{ON}^{-1}(LA) = \alpha_{LA}L + \beta_{LA}, \quad (2)$$

where α_{DA} and α_{LA} is the slope to the irradiance of the ON rate constant of the DA and LA photocurrents, respectively, and β_{DA} and β_{LA} is the light-independent component of the ON rate constant of the DA and LA photocurrents, respectively. The above relationship was different between the DA and LA photocurrents at any wavelength. In the response to blue light, α_{DA} was significantly larger than α_{LA} ($P<0.005$, n=10), whereas the difference between β_{DA} and β_{LA} was not significant (Fig. 2D and E). In response to cyan light, α_{DA} was significantly larger than α_{LA} ($P<0.005$, n=10), whereas the difference between β_{DA} and β_{LA} was not significant (Fig. 2D and E). In response to teal light, the difference between α_{DA} and α_{LA} was not significant whereas β_{DA} was significantly larger than β_{LA} ($P<0.05$, n=10, Fig. 2D and E).

On the other hand, the OFF rate constants of both DA and LA, τ_{OFF}^{-1}(DA) and τ_{OFF}^{-1}(LA), were almost independent on the irradiance at all wavelengths (Fig. 3A–C). Although they seemed to be somewhat negatively related to the teal irradiance, the differences were not statistically significant (n=10, Kruskal-Wallis test of ANOVA). This negative relationship may be attributed to the increasing contribution of desensitization during test pulse of 20 or 100 ms as the rate of desensitization is dependent on the irradiance. Thus the extrapolated values to 0 irradiance were used as the τ_{OFF}^{-1}(DA) and τ_{OFF}^{-1}(LA) estimates in the following experiments. As shown in Figure 3D, τ_{OFF}^{-1}(LA) was significantly larger than τ_{OFF}^{-1}(DA) at blue ($P<0.005$, n=10) and cyan ($P<0.005$, n=10).

Comparison of ON kinetics among ChR1/2 chimeras

The above kinetic differences between the DA and LA photocurrents should be attributed to the structural changes in the ChR2 protein moiety by the desensitization. To identify them, we divided the amino acid sequences of the ChR2 into seven domains "*a*"–"*g*" so that each one practically contained a single TM, and measured the kinetic parameters of the photocurrents for each ChR1/2 chimera in which some of the domains of ChR2 were replaced by their counterparts from ChR1, domains "*A*"–"*G*" (Supplementary Fig. S1) producing five chimeras, ChR-*Abcdefg*, ChR-*ABcdefg*, ChR-*ABCdefg*, ChR-*ABCDefg* and ChR-*ABCDEfg* [11].

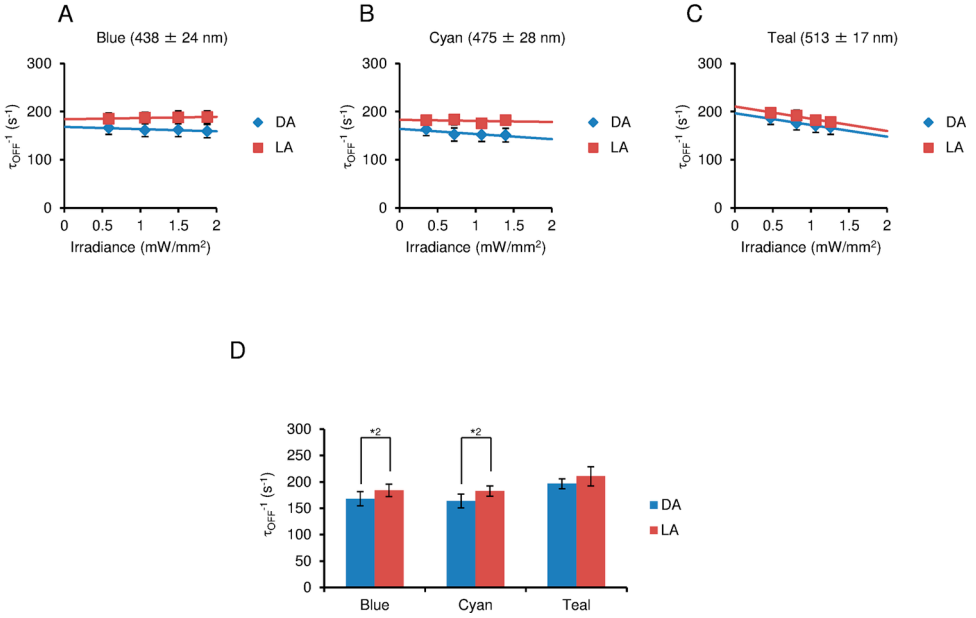

Figure 3 Desensitization-dependent changes of the OFF kinetics. (A)–(C) The relationship between the OFF rate constant (τ_{OFF}^{-1}) and the irradiance of the DA (blue symbols) and LA (red symbols) photocurrents with blue (A, n=10), cyan (B, n=10) and teal (C, n=10). (D) The comparison of τ_{OFF}^{-1} between DA and LA photocurrents with blue (n=10), cyan (n=10) and teal (n=10). Wilcoxon signed rank test: *1 (P<0.05), *2 (P<0.005).

The photocurrent could not be analyzed for ChR1 and ChR-*ABCDEFg* because of the low amplitude and signal/noise ratio. For each of the chimeras, the ON rate constants, τ_{ON}^{-1}(DA) and τ_{ON}^{-1}(LA), followed a linear function of *L*, whereas the OFF rate constants, τ_{OFF}^{-1}(DA) and τ_{OFF}^{-1}(LA), were not dependent on *L*. The slopes to the irradiance, α_{DA}, α_{LA} were varied among the chimeras. As shown in Figure 4A, a significant decrease in α_{DA} was induced by exchanging the domain "*a*" of ChR2 with the counterpart of ChR1 (domain "*A*") at all wavelengths. However, it was significantly increased by addition of the "*b*"-to-"*B*" exchange with blue and teal. Similarly the "*d*"-to-"*D*" exchange significantly decreased α_{DA} at all wavelengths, whereas the "*c*"-to-"*C*" and "*e*"-to-"*E*" did not. The differences between α_{DA} and α_{LA} are expressed by the α_{LA}/α_{DA} ratio as shown in Figure 4B. For all chimeras, the α_{LA}/α_{DA} ratio was generally significantly smaller than 1.0 at all wavelengths. However, the change was insignificant for ChR2 with teal and for ChR-*ABCDefg* with blue and cyan. To test change in the spectral sensitivity by the desensitization, the ratio of α_{DA} (or α_{LA}) with blue over that with cyan (B/C ratio) and the ratio of α_{DA} (or α_{LA}) with teal over that with cyan (T/C ratio) were compared between the DA and LA photocurrents (Fig. 5). Although neither of the ratios of B/C and T/C was significantly changed for ChR2, a significant reduction of the T/C ratio was observed by the light adaptation for the other chimeras (ChR-*Abcdefg*, -*ABcdefg*, -*ABCdefg*, -*ABCDefg* and -*ABCDEfg*). The B/C ratio was also significantly reduced for ChR-*ABcdefg*.

Next, the light-independent components, β_{DA} and β_{LA}, were

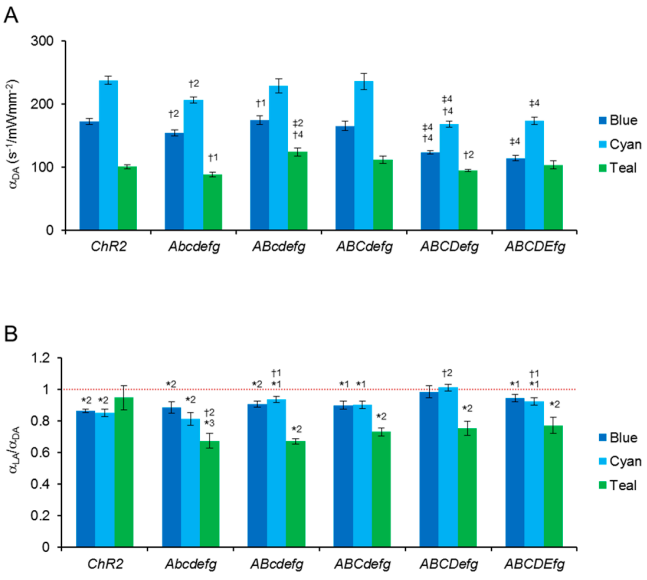

Figure 4 Comparison of α_{DA} and α_{LA} among (from left to right) ChR2 and ChR1/2 chimeras. (A) α_{DA} of ChR2 (blue, n=10; cyan, n=10; teal, n=10), ChR-*Abcdefg* (blue, n=12; cyan, n=11; teal, n=12), ChR-*ABcdefg* (blue, n=10; cyan, n=9; teal, n=11), ChR-*ABCdefg* (blue, n=9; cyan, n=10; teal, n=9), ChR-*ABCDefg* (blue, n=11; cyan, n=11; teal, n=10) and ChR-*ABCDEfg* (blue, n=11; cyan, n=11; teal, n=11). (B) The α_{LA}/α_{DA} ratio. Wilcoxon signed rank test between DA and LA photocurrents: *1 (P<0.05), *2 (P<0.005), *3 (P<0.0005). Mann-Whitney *U*-test between neighbors: †1 (P<0.05), †2 (P<0.005), †4 (P<0.00005) and between ChR2 and ChR1/2 chimeras: ‡2 (P<0.005), ‡4 (P<0.00005).

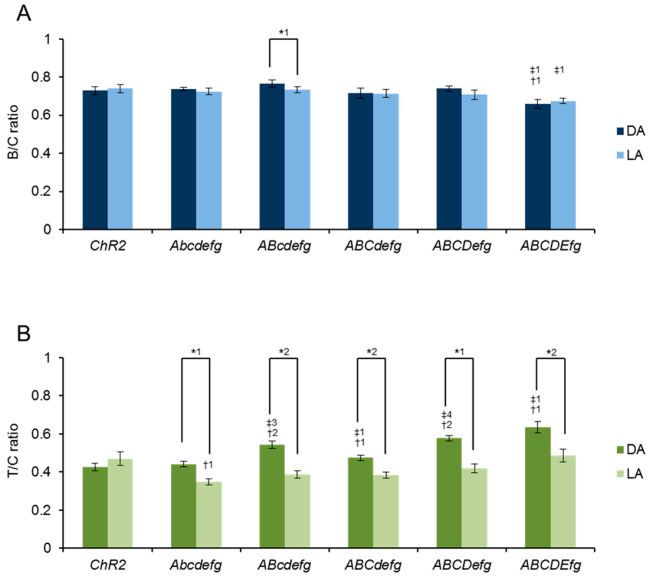

Figure 5 Comparison of the spectral sensitivity among (from left to right) ChR2 (n=10), ChR-*Abcdefg* (n=9), ChR-*ABcdefg* (n=9), ChR-*ABCdefg* (n=9), ChR-*ABCDefg* (n=9) and ChR-*ABCDEfg* (n=9). (A) The ratio of α_{DA} (dark blue columns) or α_{LA} (light blue columns) with blue compared to that with cyan (B/C ratio). (B) The ratio of α_{DA} (dark green columns) or α_{LA} (light green columns) with teal compared to that with cyan (T/C ratio). Wilcoxon signed rank test between DA and LA photocurrents: ^{*1} ($P<0.05$), ^{*2} ($P<0.005$). Mann-Whitney *U*-test between neighbors: ^{†1} ($P<0.05$), ^{†2} ($P<0.005$) and between ChR2 and ChR1/2 chimeras: ^{‡1} ($P<0.05$), ^{‡3} ($P<0.0005$), ^{‡4} ($P<0.00005$).

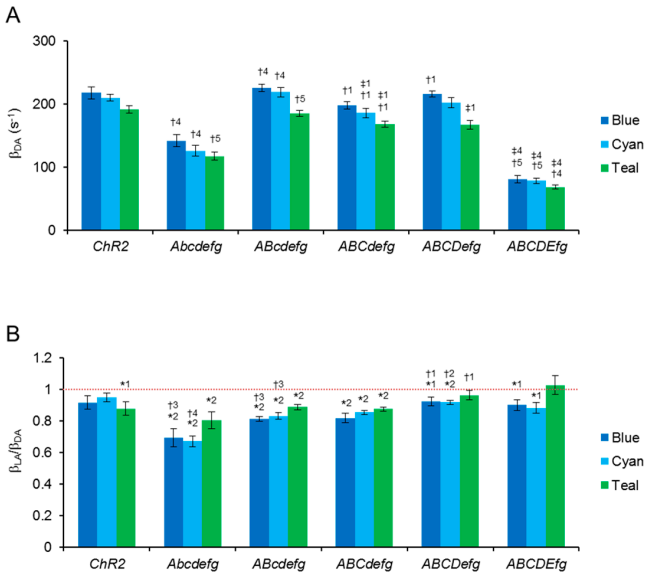

Figure 6 Comparison of β_{DA} and β_{LA} among (from left to right) ChR2 and ChR1/2 chimeras. (A) β_{DA} of ChR2 (blue, n=10; cyan, n=10; teal, n=10), ChR-*Abcdefg* (blue, n=12; cyan, n=11; teal, n=12), ChR-*ABcdefg* (blue, n=10; cyan, n=9; teal, n=11), ChR-*ABCdefg* (blue, n=9; cyan, n=10; teal, n=9), ChR-*ABCDefg* (blue, n=11; cyan, n=11; teal, n=10) and ChR-*ABCDEfg* (blue, n=11; cyan, n=11; teal, n=11). (B) The β_{LA}/β_{DA} ratio. Wilcoxon signed rank test between DA and LA photocurrents: ^{*1} ($P<0.05$), ^{*2} ($P<0.005$). Mann-Whitney *U*-test between neighbors: ^{†1} ($P<0.05$), ^{†2} ($P<0.005$), ^{†3} ($P<0.0005$), ^{†4} ($P<0.00005$), ^{†5} ($P<0.000005$) and between ChR2 and ChR1/2 chimeras: ^{‡1} ($P<0.05$), ^{‡4} ($P<0.00005$).

compared among the chimeras. As shown in Figure 6A, the "*a*"-to-"*A*" exchange of ChR2 significantly decreased β_{DA}, whereas the additional "*b*"-to-"*B*" exchange significantly increased it at all wavelengths. Similarly, the "*c*"-to-"*C*" and "*e*"-to-"*E*" exchanges significantly decreased it. The effect of the "*d*"-to-"*D*" exchange was significant only with blue. The difference between β_{DA} and β_{LA} are expressed by the β_{LA}/β_{DA} ratio, as shown in Figure 6B. For all the chimeras, the β_{LA}/β_{DA} ratio was generally significantly smaller than 1.0 at all wavelengths. However, the change was insignificant for ChR2 with blue and cyan and for ChR-*ABCDefg* and ChR-*ABCDEfg* with teal.

Comparison of OFF kinetics among ChR1/2 chimeras

The OFF rate constants (τ_{OFF}^{-1}) varied among the chimeras but were dependent on neither the wavelength nor irradiance (Fig. 7A). Particularly, it was significantly decreased by the "*a*"-to-"*A*" and the "*e*"-to-"*E*" exchanges and significantly increased by the "*b*"-to-"*B*" at all wavelengths. The decreasing effects of "*c*"-to-"*C*" exchange and the increasing effect of "*d*"-to-"*D*" exchanges were also significant with blue and cyan. The differences between τ_{OFF}^{-1}(DA) and τ_{OFF}^{-1}(LA) are expressed by the τ_{OFF}^{-1}(LA)/τ_{OFF}^{-1}(DA) ratio as shown in Figure 7B. As noted previously (Fig. 3D), τ_{OFF}^{-1}(LA) was significantly larger than τ_{OFF}^{-1}(DA) with blue and cyan for ChR2. On the other hand, the τ_{OFF}^{-1}(LA)/τ_{OFF}^{-1}(DA) ratio was significantly less than 1.0 for ChR-*Abcdefg*, -*ABcdefg* and -*ABCdefg* at all wavelengths as well as for ChR-*ABCDefg* with cyan. The effects of desensitization were almost negligible for ChR-*ABCDefg* with blue and teal and for -*ABCDEfg* at all wavelengths.

Although τ_{OFF}^{-1}(DA) was significantly smaller than β_{DA} with blue for ChR2 ($P<0.05$), ChR-*Abcdefg* ($P<0.0005$), ChR-*ABcdefg* ($P<0.005$), ChR-*ABCdefg* ($P<0.005$), ChR-*ABCDefg* ($P<0.005$) and ChR-*ABCDEfg* ($P<0.005$), the averaged values showed high correlation ($r=0.99$), as shown in Figure 8A. This relationship was similar with cyan ($r=0.99$). The averaged values were almost coincident with teal ($r=0.99$) and with insignificant differences except for ChR-*ABCDefg*, in which τ_{OFF}^{-1}(DA) was significantly larger than β_{DA} ($P<0.005$). A similar correlation was observed between τ_{OFF}^{-1}(LA) and β_{LA} with blue ($r=1.00$), cyan ($r=1.00$) and teal ($r=0.98$) (Fig. 8D–F). Although τ_{OFF}^{-1}(LA) was again smaller than β_{LA} for ChR-*ABCDEfg* ($P<0.05$) with blue and for ChR-*ABcdefg* ($P<0.05$) and -*ABCdefg* ($P<0.05$) with cyan, both values were almost coincident witht teal except for ChR2 ($P<0.05$).

Discussion

Previously, multiple-photocycle models were proposed to account for the photocurrent kinetics and spectroscopic

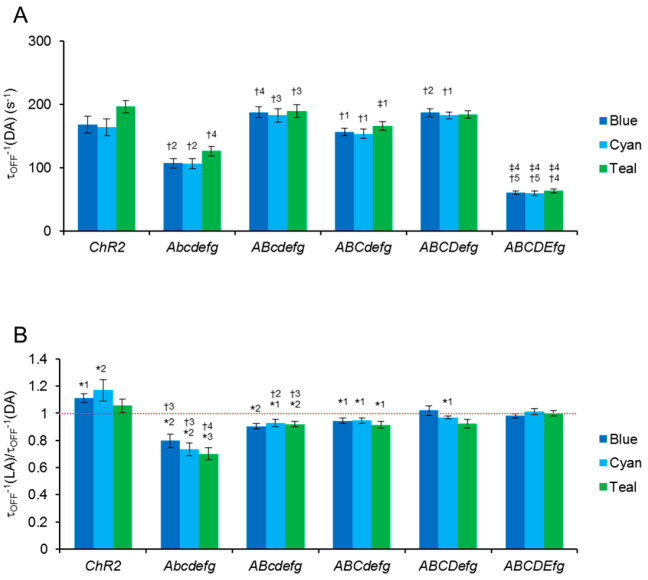

Figure 7 Comparison of the OFF rate constants, τ_{OFF}^{-1}(DA) and τ_{OFF}^{-1}(LA) among (from left to right) ChR2 and ChR1/2 chimeras. (A) τ_{OFF}^{-1}(DA) of ChR2 (blue, n=10; cyan, n=10; teal, n=10), ChR-*Abcdefg* (blue, n=12; cyan, n=11; teal, n=12), ChR-*ABcdefg* (blue, n=10; cyan, n=9; teal, n=11), ChR-*ABCdefg* (blue, n=9; cyan, n=10; teal, n=9), ChR-*ABCDefg* (blue, n=11; cyan, n=11; teal, n=10) and ChR-*ABCDEfg* (blue, n=11; cyan, n=11; teal, n=11). (B) The t_{OFF}^{-1}(LA)/t_{OFF}^{-1}(DA) ratio. Wilcoxon signed rank test between DA and LA photocurrents: ^{*1} (P<0.05), ^{*2} (P<0.005) , ^{*3} (P<0.0005). Mann-Whitney *U*-test between neighbors: $^{\dagger 1}$ (P<0.05), $^{\dagger 2}$ (P<0.005), $^{\dagger 3}$ (P<0.0005), $^{\dagger 4}$ (P<0.00005), $^{\dagger 5}$ (P<0.000005) and between ChR2 and ChR1/2 chimeras: $^{\ddagger 1}$ (P<0.05), $^{\ddagger 4}$ (P<0.00005).

transitions of various ChRs [7,10,14,15–20]. That is, there should be at least two ground states (D_1, D_2) and two open states (O_1, O_2) [6,7,16]. When a flash of light is applied to a ChR-expressing cell under dark adaptation, some molecules enter the cation-conducting state (O_1) to generate a photocurrent under whole-cell voltage clamp of the cell (Fig. 9). As the O_1 is relatively unstable, the molecules become non-conductive with a certain probability and reactivated again through D_1. However, some of them have different conformations of D_2 and, with a certain probability, go into the independent desensitized photocycle with a different cation-conducting state (O_2). With a smaller average conductance for O_2 than O_1, the photocurrent is progressively attenuated in amplitude. Finally, most of the molecules enter the desensitized photocycle with a steady-state plateau photocurrent as the recovery rate from D_2 to D_1 is relatively slow [2,8,9]. The present study provides the additional evidence of this multiple-photocycle model, that is, the D_1-O_1-D_1 photocycle and the D_2-O_2-D_2 photocycle are kinetically distinct. The τ_{ON}^{-1}(DA) of ChR2 was consistently larger than the τ_{ON}^{-1}(LA) for the same irradiance at a given wavelength. On the other hand, the τ_{OFF}^{-1}(DA) of ChR2 was consistently smaller than the corresponding τ_{OFF}^{-1}(LA).

In the present study, it was experimentally demonstrated that the turning-on rate (τ_{ON}^{-1}) of the DA/LA photocurrent is linearly related to a relatively wide range of irradiance (*L*), as previously noted [21–23]. This is consistent with the two-state model prediction that the transition from basal (D_1/D_2) to conductive states (O_1/O_2) is approximated by a single-photon reaction and the transition from conductive (O_1/O_2) to basal states (D_1/D_2) is a light-independent thermal reaction. That is,

$$\tau_{ON}^{-1}(D_1 \rightarrow O_1) = \varepsilon_1 \varphi_1 L + \beta_1, \quad (3)$$

$$\tau_{OFF}^{-1}(O_1 \rightarrow D_1) = \beta_1, \quad (4)$$

$$\tau_{ON}^{-1}(D_2 \rightarrow O_2) = \varepsilon_2 \varphi_2 L + \beta_2, \quad (5)$$

and

$$\tau_{OFF}^{-1}(O_2 \rightarrow D_2) = \beta_2, \quad (6)$$

where the constants ε_1 and ε_2 are respectively the molar absorption coefficient equivalents of D_1 and D_2, and are determinants of the spectral sensitivity of each state [24]. The constants φ_1 and φ_2 are respectively the quantum yield equivalents of D_1 and D_2. The φ_1 is proportional to the probability of a molecule to change its conformation from D_1 to O_1, whereas the φ_2 is proportional to the probability of a state transition from D_2 to O_2. The constants β_1 and β_2 are independent of *L*, but are dependent on the probability of the molecule to return from conductive (O_1 and O_2) to basal states (D_1 and D_2). In the present study, each steepness, $\varepsilon_1\varphi_1$ and $\varepsilon_2\varphi_2$, was experimentally approximated by α_{DA} and α_{LA}, and each constant, β_1 and β_2, was approximated either by β_{DA} and β_{LA} or by τ_{OFF}^{-1}(DA) and τ_{OFF}^{-1}(LA), which were directly measured from the photocurrents. These values would give us some insight into differences in the molecular dynamics between non-desensitized and desensitized photocycles and would also be key parameters for predicting the photocurrent kinetics of ChR as a function of irradiance (*L*) and time.

Deceleration of ChR2 kinetics by desensitization

In the case of ChR2, the α_{LA} was smaller than α_{DA} with blue and cyan (Figs. 2D and 4B) and without changes in the B/C and T/C ratios (Fig. 5A and 5B). Therefore, it could be predicted that φ_2 is smaller than φ_1 whereas ε_1 and ε_2 are similar. The insignificant difference in α_{LA} and α_{DA} with teal suggest that the difference between φ_1 and φ_2 may be cancelled by the small difference between ε_1 and ε_2. Similarly, β_{LA} tended to be smaller than β_{DA}, but the difference was significant only with teal (Figs. 2E and 6B). This could be attributed to the fact that β_{DA} overestimated β_1 because of the relatively fast rate of desensitization with blue and cyan. Therefore, it is suggested that both probabilities from the basal to conductive states and from the conductive to basal states are decreased by the desensitization. However, this is somewhat conflicts with the fact that τ_{OFF}^{-1}(LA) of ChR2 was larger than τ_{OFF}^{-1}(DA) with blue and cyan (Fig. 3D) as τ_{OFF}^{-1}(LA) should be proportional to the probability of a channel to close.

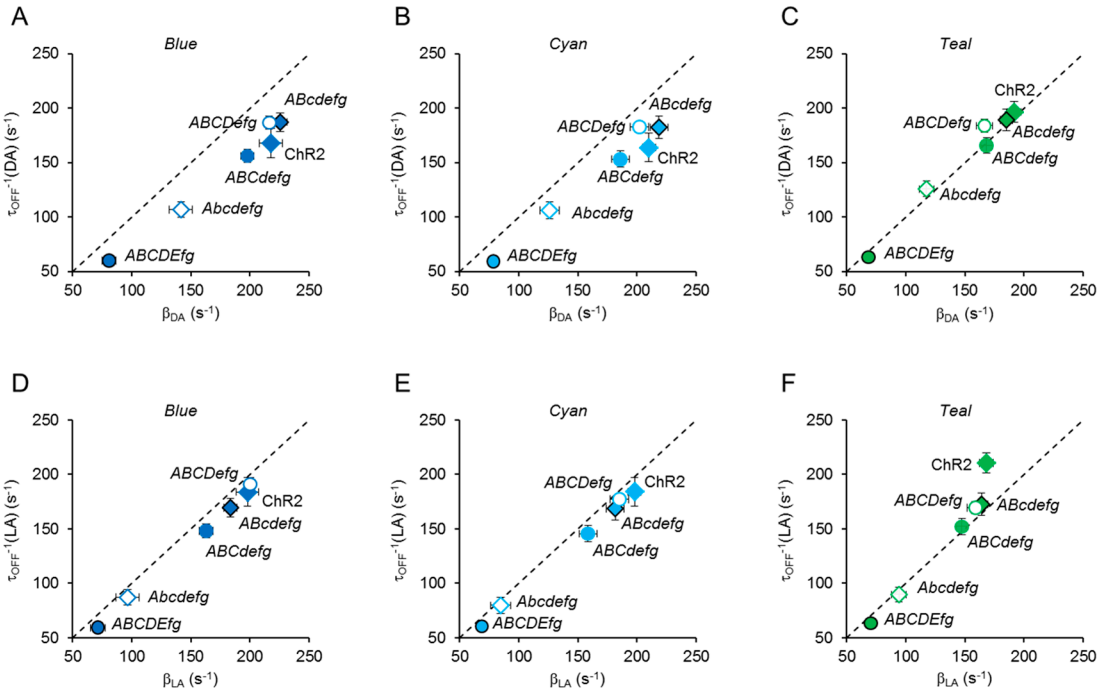

Figure 8 Correlation between τ_{OFF}^{-1} and β. Each symbol is the mean±SEM for ChR2 (blue, n=10; cyan, n=10; teal, n=10), ChR-*Abcdefg* (blue, n=12; cyan, n=11; teal, n=12), ChR-*ABcdefg* (blue, n=10; cyan, n=9; teal, n=11), ChR-*ABCdefg* (blue, n=9; cyan, n=10; teal, n=9), ChR-*ABCDefg* (blue, n=11; cyan, n=11; teal, n=10) and ChR-*ABCDEfg* (blue, n=11; cyan, n=11; teal, n=11). (A)–(C) Relationship between τ_{OFF}^{-1}(DA) and β_{DA} with blue, cyan and teal, respectively. (D)–(F) Relationship between τ_{OFF}^{-1}(LA) and β_{LA} with blue, cyan and teal, respectively.

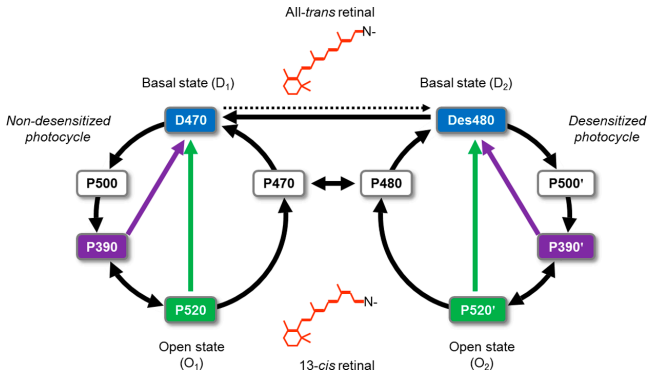

Figure 9 Two-photocycle model of channelrhodopsin. The non-desensitized photocycle starts from the dark-adapted basal state (D_1) to the open/cation-conducting state (O_1) through intermediates (P 500 and P 390) with a relatively short dwelling time. The desensitized photocycle is similar, but starts from the light-adapted basal state (D_2) to the open/cation-conducting state (O_2) with a different conductance. The transition from D_2 to D_1 is relatively slow compared to the photocycle period.

Evaluation of the TM exchanges

We found that ChR2 and ChR1/2 chimeras differed even in the kinetics of the DA photocurrents as reported previously [11,12]. These differences could be attributed to structural changes of the opsins. Although the "*a*"-to-"*A*" exchange of ChR2 did not affect the spectral sensitivity (Fig. 5A and 5B), it decreased α_{DA} (Fig. 4A), β_{DA} (Fig. 6A) and τ_{OFF}^{-1}(DA) (Fig. 7A) at all wavelengths, suggesting that the probabilities of D_1-O_1 and O_1-D_1 transition are dependent on the TM1. This domain should also be involved in the desensitization-dependent change of spectral sensitivity (Fig. 5B) as well as the desensitization-dependent reduction of the probabilities of state transitions during a photocycle. Particularly, the deceleration of the O_2-D_2 transition became manifest with the decrease of β_{LA}/β_{DA} (Fig. 6B) and $\tau_{OFF}^{-1}(LA)/\tau_{OFF}^{-1}(DA)$ (Fig. 7B). The further "*b*"-to-"*B*" exchange increased α_{DA} (Fig. 4A), β_{DA} (Fig. 6A) and τ_{OFF}^{-1}(DA) (Fig. 7A), suggesting that the probabilities of the D_1-O_1 and O_1-D_1 transition are also dependent on the TM2. Although the magnitude was decreased, the reduction of the state transition probability remained (Figs. 4B, 6B and 7B). The spectral sensitivity appeared to be red-shifted further by this exchange (Fig. 5B) with a significant reduction of the B/C ratio by desensitization (Fig. 5A). On the other hand, the effects of the "*c*"-to-"*C*" exchange were negligible for α_{DA} (Fig. 4A) although its desensitization-dependent change remained (Fig. 4B). However, β_{DA} and τ_{OFF}^{-1}(DA) were significantly reduced (Figs. 6A and 7A), the T/C ratio was reduced in the DA photocurrent (Fig. 5B) and the B/C ratio became insensitive to desensitization again (Fig. 5A) even though a single amino acid, Ser^{181}, in "*c*" was Ala in "*C*". The effects of the "*d*"-to-"*D*" exchange were also considerably manifest particularly for α_{DA} (Fig. 4A), with the

enhanced T/C ratio at DA photocurrent (Fig. 5B) although TM4 is highly conserved and only 7 amino acids are different. In this chimera, ChR-*ABCDefg*, the effects of desensitization were smaller than in the others; the difference between α_{DA} and α_{LA} was negligible with blue and cyan (Fig. 4B), that between β_{DA} and β_{LA} was negligible with teal (Fig. 6B) and that between τ_{OFF}^{-1}(DA) and τ_{OFF}^{-1}(LA) was negligible at all wavelengths (Fig. 7B). In contrast, the "*e*"-to-"*E*" exchange reduced β_{DA} and τ_{OFF}^{-1}(DA) (Figs. 6A and 7A) with a significant red-shift of the DA photocurrent (Fig. 5A and 5B). Although its effect on α_{DA} was insignificant at any wavelength (Fig. 4A), it induced a desensitization-dependent attenuation of the basal-to-conductive state transition (Fig. 4B).

As a general rule common to chimeras, high correlations were present between β_{DA} and τ_{OFF}^{-1}(DA) as well as between β_{LA} and τ_{OFF}^{-1}(LA) (Fig. 8). Therefore, the simple two-state model (equations (3)–(6)) may approximate the ON/OFF kinetics. However, τ_{OFF}^{-1}(DA) was significantly smaller than β_{DA} with blue and cyan. This is probably due to the increasing contribution of desensitization during the first test pulse of light (20 ms) to measure τ_{OFF}^{-1}(DA) as the rate of desensitization with blue and cyan was larger than that with teal at the same irradiance. Indeed, τ_{OFF}^{-1}(DA) was almost equal to β_{DA} when the test light pulse was short (10 ms) (Supplementary Fig. S3). However, the distinctive trait of ChR-*ABCDefg*, that τ_{OFF}^{-1}(DA) was significantly larger than β_{DA} with teal, and the trait of ChR2, that τ_{OFF}^{-1}(LA) was significantly larger than β_{LA} with teal, has to be otherwise explained.

Molecular dynamics of desensitization

In summary, both the D_1 to O_1 and D_2 to O_2 state transitions are suggested to be regulated by the interaction between TM1 and TM2 and are decelerated by the heterogeneous combination of "*A*" and "*b*". These transitions are also dependent on the TM4. Similarly, the O_1 to D_1 and O_2 to D_2 state transitions are suggested to be regulated by the interaction between TM1 and TM2, although not by TM4. On the other hand these transitions are both dependent on TM5. Probably, TM1 and 2 are involved in the general stabilization of the molecule, whereas the translocation of TM4 may contribute to the stabilization of D_1 and D_2, and TM5 may contribute the stabilization of O_1 and O_2. Indeed, Gln^{95}, Thr^{98} and Ser^{102} in the TM1 of C1C2, the ChR-*ABCDEfg* equivalent, and the five Glu (Glu^{121}, Glu^{122}, Glu^{129}, Glu^{136}, Glu^{140}) and Lys^{132} in TM2 (C1C2) have been suggested to form a hydrophilic channel with the amino acids in TM3 [5,21,22,25]. This notion is consistent with a recent molecular dynamics simulation showing that the movements of TM6, 7 and 2 are induced by the photoisomerization of retinal [26]. These conformational changes of the opsins are presumed to be almost similar for desensitized photocycles although the desensitization may cause the stabilization of both D_2 and O_2. It is possible that the more destabilized basal state in the non-desensitized photocycle, that is, the fact that $\varphi_1 > \varphi_2$, is the consequence of the isomerization of all-*trans*, 15-*anti*-form of retinal to 13-*cis*, 15-*syn*-form in darkness [16] although no significant change in the spectral sensitivity of ChR2 was observed in the present study (Fig. 5).

The spectral sensitivity of a rhodopsin, either animal or microbial type, is influenced by a number of factors. Among them, the interaction between the retinal chromophore and the counterions around it are suggested to be critical [6,27]. That is, the negative charge distribution near the retinal-Schiff base (RSB^+) stabilizes the basal state to blue-shift the spectrum. On the other hand, the negative charge distribution near the β-ionone ring red-shifts the spectrum. Although the position of TM1 is remote from the chromophore in C1C2 [5] and indeed its exchange from ChR2 to ChR1 showed no obvious influence on the spectral sensitivity, this exchange significantly induced the desensitization-dependent blue shift. A crystallographic study indicated that TM1 lies closer to the RSB^+ than the β-ionone ring in C1C2 [5]. Therefore, the desensitization might move some negative amino acids in "*A*" such as Glu^{87}, which is neutral Ala in ChR2, towards RSB^+ by the translocation/de-protonation or other positive amino acids such as Lys^{88}, which is neutral Gln in ChR2, away from RSB^+. Alternatively, the interaction of TM1 of ChR1 and TM2 (ChR1 or 2) may change the charge distribution around RSB^+ in desensitized ChR, since a small but significant reduction of the B/C ratio by desensitization was observed only for ChR2-*ABcdefg*. These two features of desensitization, stabilization of the protein conformation and a change in the charge distribution around RSB^+, could be generated by the same structure, such as the H-bond formation between TM1 and other TMs. Indeed, Thr^{98} in TM1 affects the position of Glu^{129} in TM2, which should be involved in the pore constriction, through Ser^{102} (TM1) and Asn^{297} (TM7) [5]. Although the precise molecular dynamics underlying this transition should be investigated in the future through spectroscopy, X-ray crystallography, site-directed mutagenesis as well as the electrophysiology in combination, a previous Fourier transform infrared (FTIR) spectroscopic study suggested that the gating and desensitizing processes in ChR1/2 chimeras are different from those in ChR2 [28].

Conclusion

The desensitization of ChR was revealed to be accompanied by a deceleration of the state transition and by a spectral shift. TM1 and 2 are the main structures involved in the desensitization-dependent change of ChR.

Acknowledgements

We thank B. Bell for language assistance. This study was supported by a Grant-in-Aid for Scientific Research (No. 25250001 to HY and No. 25290002 to TI) from the Ministry of Education, Culture, Sports, Science and Technology (MEXT) of Japan, a Grant-in-Aid for Scientific Research on

Innovative Areas “Adaptive Circuit Shift” (No. 15H01413 to HY) of the Ministry of Education, Culture, Sports, Science and Technology (MEXT) of Japan, a Grant-in-Aid for challenging Exploratory Research (No. 15K15025 to HY), MEXT of Japan and JST, Strategic International Collaborative Research Program, SICORP.

Conflict of Interest

A. Z., S. S., T. I. and H. Y. declare that they have no conflict of interest.

Author Contributions

A. Z. and S. S. performed most of the experiments and analysis. T. I. and H. Y. directed the entire project and cowrote the manuscript.

References

[1] Nagel, G., Ollig, D., Fuhrmann, M., Kateriya, S., Musti, A. M., Bamberg, E., *et al.* Channelrhodopsin-1: a light-gated proton channel in green algae. *Science* **296**, 2395–2398 (2002).

[2] Nagel, G., Szellas, T., Huhn, W., Kateriya, S., Adeishvili, N., Berthold, P., *et al.* Channelrhodopsin-2, a directly light-gated cation-selective membrane channel. *Proc. Natl. Acad. Sci. USA* **100**, 13940–13945 (2003).

[3] Sineshchekov, O. A., Jung, K.-H. & Spudich, J. L. Two rhodopsins mediate phototaxis to low- and high-intensity light in *Chlamydomonas reinhardtii*. *Proc. Natl. Acad. Sci. USA* **99**, 8689–8694 (2002).

[4] Suzuki, T., Yamasaki, K., Fujita, S., Oda, K., Iseki, M., Yoshida, K., *et al.* Archaeal-type rhodopsins in *Chlamydomonas*: model structure and intracellular localization. *Biochem. Biophys. Res. Commun.* **301**, 711–717 (2003).

[5] Kato, H. E., Zhang, F., Yizhar, O., Ramakrishnan, C., Nishizawa, T., Hirata, K., *et al.* Crystal structure of the channelrhodopsin light-gated cation channel. *Nature* **482**, 369–374 (2012).

[6] Ernst, O. P., Lodowski, D. T., Elstner, M., Hegemann, P., Brown, L. S. & Kandori, H. Microbial and animal rhodopsins: structures, functions, and molecular mechanisms. *Chem. Rev.* **114**, 126–163 (2014).

[7] Lórenz-Fonfría, V. A. & Heberle, J. Channelrhodopsin unchained: structure and mechanism of a light-gated cation channel. *Biochim. Biophys. Acta* **1837**, 626–642 (2014).

[8] Ishizuka, T., Kakuda, M., Araki, R. & Yawo, H. Kinetic evaluation of photosensitivity in genetically engineered neurons expressing green algae light-gated channels. *Neurosci. Res.* **54**, 85–94 (2006).

[9] Mattis, J., Tye, K. M., Ferenczi, E. A., Ramakrishnan, C., O’Shea, D. J., Prakash, R., *et al.* Principles for applying optogenetic tools derived from direct comparative analysis of microbial opsins. *Nat. Methods* **9**, 159–172 (2012).

[10] Hegemann, P., Ehlenbeck, S. & Gradmann, D. Multiple photocycles of channelrhodopsin. *Biophys. J.* **89**, 3911–3918 (2005).

[11] Wang, H., Sugiyama, Y., Hikima, T., Sugano, E., Tomita, H., Takahashi, T., *et al.* Molecular determinants differentiating photocurrent properties of two channelrhodopsins from *Chlamydomonas*. *J. Biol. Chem.* **284**, 5685–5696 (2009).

[12] Wen, L., Wang, H., Tanimoto, S., Egawa, R., Matsuzaka, Y., Mushiake, H., *et al.* Opto-current-clamp actuation of cortical neurons using a strategically designed channelrhodopsin. *PLoS ONE* **5**, e12893 (2010).

[13] Watanabe, S., Ishizuka, T., Hososhima, S., Zamani, A., Hoque, M. R., Yawo, H. The regulatory mechanism of ion permeation through a channelrhodopsin derived from *Mesostigma viride* (MvChR1). *Photochem. Photobiol. Sci.* **15**, 365–374 (2016).

[14] Yawo, H., Asano, T., Sakai, S. & Ishizuka, T. Optogenetic manipulation of neural and non-neural functions. *Dev. Growth. Differ.* **55**, 474–490 (2013).

[15] Ernst, O. P., Sánchez Murcia, P. A., Daldrop, P., Tsunoda, S. P., Kateriya. S. & Hegemann, P. Photoactivation of channelrhodopsin. *J. Biol. Chem.* **283**, 1637–1643 (2008).

[16] Stehfest, K., Ritter, E., Berndt, A., Bartl, F. & Hegemann, P. The branched photocycle of the slow-cycling channelrhodopsin-2 mutant C128T. *J. Mol. Biol.* **398**, 690–702 (2010).

[17] Nikolic, K., Grossman, N., Grubb, M. S., Burrone, J., Toumazou, C. & Degenaar, P. Photocycles of channelrhodopsin-2. *Photochem. Photobiol.* **85**, 400–411 (2009).

[18] Ritter, E., Piwowarski, P., Hegemann, P. & Bartl, F. J. Light-dark adaptation of channelrhodopsin C128T mutant. *J. Biol. Chem.* **288**, 10451–10458 (2013).

[19] Ritter, E., Stehfest, K., Berndt, A., Hegemann, P. & Bartl, F. J. Monitoring light-induced structural changes of Channelrhodopsin-2 by UV-visible and Fourier transform infrared spectroscopy. *J. Biol. Chem*. **283**, 35033–35041 (2008).

[20] Stehfest, K. & Hegemann, P. Evolution of the channelrhodopsin photocycle model. *Chemphyschem* **11**, 1120–1126 (2010).

[21] Sugiyama, Y., Wang, H., Hikima, T., Sato, M., Kuroda, J., Takahashi, T., *et al.* Photocurrent attenuation by a single polar-to-nonpolar point mutation of channelrhodopsin-2. *Photochem. Photobiol. Sci.* **8**, 328–336 (2009).

[22] Tanimoto, S., Sugiyama, Y., Takahashi, T., Ishizuka, T. & Yawo, H. Involvement of glutamate 97 in ion influx through photo-activated channelrhodopsin-2. *Neurosci. Res.* **75**, 13–22 (2013).

[23] Yawo, H., Tanimoto, S., Ishizuka, T. & Takahashi, T. Molecular dynamics of photo-electrical transducing proteins, channelrhodopsins. *Seibutsu Butsuri* **52**, 226–229 (2013).

[24] Hososhima, S., Sakai, S., Ishizuka, T. & Yawo, H. Kinetic evaluation of photosensitivity in bi-stable variants of chimeric channelrhodopsins. *PLoS ONE* **10**, e0119558 (2015).

[25] Plazzo, A. P., De Franceschi, N., Da Broi, F., Zonta, F., Sanasi, M. F., Filippini, F., *et al.* Bioinformatic and mutational analysis of channelrhodopsin-2 protein cation-conducting pathway. *J. Biol. Chem.* **287**, 4818–425 (2012).

[26] Takemoto, M., Kato, H. E., Koyama, M., Ito, J., Kamiya, M., Hayashi, S., *et al.* Molecular dynamics of channelrhodopsin at the early stages of channel opening. *PLoS ONE* **10**, e0131094 (2015).

[27] Zhang, F., Prigge, M., Beyrière, F., Tsunoda, S. P., Mattis, J., Yizhar, O., *et al.* Red-shifted optogenetic excitation: a tool for fast neural control derived from *Volvox carteri*. *Nat. Neurosci.* **11**, 631–633 (2008).

[28] Inaguma, A., Tsukamoto, H., Kato, H. E., Kimura, T., Ishizuka, T., Oishi, S., *et al.* Chimeras of channelrhodopsin-1 and -2 from *Chlamydomonas reinhardtii* exhibit distinctive light-induced structural changes from channelrhodopsin-2. *J. Biol. Chem.* **290**, 11623–11634 (2015).